Bending Vibration-Governed Solvation Dynamics of an Excess Electron in Liquid Acetonitrile Revealed by Ab Initio Molecular Dynamics Simulation

Jinxiang Liu,[†] Robert I. Cukier,[‡] Yuxiang Bu [†,1]

[†] *School of Chemistry and Chemical Engineering, Shandong University, Jinan, 250100, P. R. China and* [‡] *Department of Chemistry, Michigan State University, East Lansing, 48824, USA.*

Supporting Information

Contents

[1] E-mail: byx@sdu.edu.cn

1. References for Utilization of Acetonitrile Molecules

[1] Chaban VV, Voroshylova IV, Kalugin ON, Prezhdo OV (2012) Acetonitrile boosts conductivity of imidazolium ionic liquids. *J Phys Chem B* 116(26):7719-7727.

[2] González CM, Pincock JA (2004) Activation energies for the singlet excited state processes of substituted benzenes: Para, meta, and ortho isomers of methylbenzonitrile and methylanisole in acetonitrile. *J Am Chem Soc* 126(29):8870-8871.

[3] McGinty RK, Kim J, Chatterjee C, Roeder RG, Muir TW (2008) Chemically ubiquitylated histone H_2B stimulates hDot1L-mediated intranucleosomal methylation. *Nature* 453(7196):812-816.

[4] Cianci M, Tomaszewski B, Helliwell JR, Halling PJ (2010) Crystallographic analysis of counterion effects on subtilisin enzymatic action in acetonitrile. *J Am Chem Soc* 132(7):2293-2300.

[5] Peryshkov DV, Popov AA, Strauss SH (2009) Direct perfluorination of $K_2B_{12}H_{12}$ in acetonitrile occurs at the gas bubble−solution interface and is inhibited by HF. Experimental and DFT study of inhibition by protic acids and soft, polarizable anions. *J Am Chem Soc* 131(51):18393-18403.

[6] Mengesha Tefashe U, Nonomura K, Vlachopoulos N, Hagfeldt A, Wittstock G (2012) Effect of cation on dye regeneration kinetics of N719-sensitized TiO_2 films in acetonitrile-based and ionic-liquid-based electrolytes investigated by scanning electrochemical microscopy. *J Phys Chem C* 116(6):4316-4323.

[7] Maity S, Choquette KA, Flowers RA, Prasad E (2012) Effect of crown ethers on the ground and excited state reactivity of samarium diiodide in acetonitrile. *J Phys Chem A* 116(9):2154-2160.

[8] Ellis WW, Raebiger JW, Curtis CJ, Bruno JW, DuBois DL (2004) Hydricities of BzNADH, $C_5H_5Mo(PMe_3)(CO)_2H$, and $C_5Me_5Mo(PMe_3)(CO)_2H$ in acetonitrile. *J Am Chem Soc* 126(9):2738-2743.

[9] Zhu X-Q, Zhang M-T, Yu A, Wang C-H, Cheng J-P (2008) Hydride, hydrogen atom, proton, and electron transfer driving forces of various five-membered heterocyclic organic hydrides and their reaction intermediates in acetonitrile. *J Am Chem Soc* 130(8):2501-2516.

[10] Lousa D*, et al.* (2012) Interaction of counterions with subtilisin in acetonitrile: Insights from molecular dynamics simulations. *J Phys Chem B* 116(20):5838-5848.

[11] Mukai K, Kohno Y, Ouchi A, Nagaoka S-i (2012) Notable effects of metal salts on UV–Vis absorption spectra of α-, β-, γ-, and δ-tocopheroxyl radicals in acetonitrile solution. The complex formation between tocopheroxyls and metal cations. *J Phys Chem B* 116(30):8930-8941.

[12] Liu S, Fourkas JT (2012) Orientational time correlation functions for vibrational sum-frequency generation. 1. Acetonitrile. *J Phys Chem A*.

[13] Lund T, Wayner DDM, Jonsson M, Larsen AG, Daasbjerg K (2001) Oxidation potentials of α-hydroxyalkyl radicals in acetonitrile obtained by photomodulated voltammetry. *J Am Chem Soc* 123(50):12590-12595.

[14] Ehrler OT, Griffin GB, Young RM, Neumark DM (2008) Photoinduced electron transfer and solvation in iodide-doped acetonitrile clusters†. *J Phys Chem B* 113(13):4031-4037.

[15] Dawson ED, Wallen SL (2002) Probing transport and microheterogeneous solvent structure in acetonitrile−water mixtures and reversed-phase chromatographic media by NMR quadrupole relaxation. *J Am Chem Soc* 124(47):14210-14220.

[16] Fu Y, Liu L, Yu H-Z, Wang Y-M, Guo Q-X (2005) Quantum-chemical predictions of absolute standard redox potentials of diverse organic molecules and free radicals in acetonitrile. *J Am Chem Soc* 127(19):7227-7234.

[17] Li R*, et al.* (2012) Radical-involved photosynthesis of aucn oligomers from au nanoparticles and acetonitrile. *J Am Chem Soc* 134(44):18286-18294.

[18] Hassinen A*, et al.* (2012) Short-chain alcohols strip x-type ligands and quench the luminescence of PbSe and CdSe quantum dots, acetonitrile does not. *J Am Chem Soc* 134(51):20705-20712.

[19] Santoro F, Barone V, Gustavsson T, Improta R (2006) Solvent effect on the singlet excited-state lifetimes of nucleic acid bases: A computational study of 5-fluorouracil and uracil in acetonitrile and water. *J Am Chem Soc* 128(50):16312-16322.

[20] Bühl M, Sieffert N, Partouche A, Chaumont A, Wipff G (2012) Speciation of La(III) chloride complexes in water and acetonitrile: A density functional study. *Inorg Chem* 51(24):13396-13407.

[21] Hamid AM, Soliman A-R, El-Shall MS (2012) Stepwise association of hydrogen cyanide and acetonitrile with the benzene radical cation: Structures and binding energies of $(C_6H_6^{\bullet+})(HCN)_n$, n = 1–6, and $(C_6H_6^{\bullet+})(CH_3CN)_n$, n = 1–4, clusters. *J Phys Chem A*.

[22] Stoppa A, Hunger J, Hefter G, Buchner R (2012) Structure and dynamics of 1-n-alkyl-3-n-methylimidazolium tetrafluoroborate + acetonitrile mixtures. *J Phys Chem B* 116(25):7509-7521.

[23] Diao E, *et al.* (2012) Structures of the ozonolysis products and ozonolysis pathway of aflatoxin B1 in acetonitrile solution. *J Agric Food Chem* 60(36):9364-9370.

[24] Warren JJ, Mayer JM (2008) Surprisingly long-lived ascorbyl radicals in acetonitrile: Concerted proton−electron transfer reactions and thermochemistry. *J Am Chem Soc* 130(24):7546-7547.

[25] McConvey IF, Woods D, Lewis M, Gan Q, Nancarrow P (2012) The importance of acetonitrile in the pharmaceutical industry and opportunities for its recovery from waste. *Organic Process Research & Development* 16(4):612-624.

[26] Reimers JR, Hall LE (1999) The solvation of acetonitrile. *J Am Chem Soc* 121(15):3730-3744.

[27] Holm AH, Yusta L, Carlqvist P, Brinck T, Daasbjerg K (2003) Thermochemistry of arylselanyl radicals and the pertinent ions in acetonitrile. *J Am Chem Soc* 125(8):2148-2157.

[28] Bühl M, Sieffert N, Chaumont A, Wipff G (2012) Water versus acetonitrile coordination to uranyl. Effect of chloride ligands. *Inorg Chem* 51(3):1943-1952.

[29] Gao J, *et al.* (2011) Electron transfer in peptides: The influence of charged amino acids. *Angew Chem Int Ed* 50(8):1926-1930.

[30] Okamoto H, Konishi H, Satake K (2012) Fluorescence response of 3-trifluoroacetylaminophthalimide to a Li^+-I^- ion pair induced by 254 nm photolysis in acetonitrile. *Chem Commun* 48(17):2346-2348.

[31] Morales CM, Thompson WH (2011) Molecular-level mechanisms of vibrational frequency shifts in a polar liquid. *J Phys Chem B* 115(23):7597-7605.

[32] Gil-Ramírez G, Escudero-Adán EC, Benet-Buchholz J, Ballester P (2008) Quantitative evaluation of anion–π interactions in solution. *Angew Chem Int Ed* 47(22):4114-4118.

[33] Koch M, Rosspeintner A, Angulo G, Vauthey E (2012) Bimolecular photoinduced electron transfer in imidazolium-based room-temperature ionic liquids is not faster than in conventional solvents. *J Am Chem Soc* 134(8):3729-3736.

[34] Melnikov SM, Höltzel A, Seidel-Morgenstern A, Tallarek U (2012) A molecular dynamics study on the partitioning mechanism in hydrophilic interaction chromatography. *Angew Chem Int Ed* 51(25):6251-6254.

[35] Mosconi E, Selloni A, De Angelis F (2012) Solvent effects on the adsorption geometry and electronic structure of dye-sensitized TiO_2: A first-principles investigation. *J Phys Chem C* 116(9):5932-5940.

[36] Cheng L, Morrone JA, Berne BJ (2012) Structure and dynamics of acetonitrile confined in a silica nanopore. *J Phys Chem C* 116(17):9582-9593.

[37] Benedetti E, Kocsis LS, Brummond KM (2012) Synthesis and photophysical properties of a series of cyclopenta[*b*]naphthalene solvatochromic fluorophores. *J Am Chem Soc* 134(30):12418-12421.

[38] Matsubara Y, Fujita E, Doherty MD, Muckerman JT, Creutz C (2012) Thermodynamic and kinetic hydricity of ruthenium(II) hydride complexes. *J Am Chem Soc* 134(38):15743-15757.

[39] Muniz-Miranda F, Pagliai M, Cardini G, Righini R (2012) Hydrogen bond effects in the vibrational spectra of 1,3-propanediol in acetonitrile: Ab initio and experimental study. *J Chem Phys* 137(24):244501.

[40] Lange KM, *et al.* (2011) On the origin of the hydrogen-bond-network nature of water: X-ray absorption and emission spectra of water–acetonitrile mixtures. *Angewandte Chemie* 123(45):10809-10813.

2. Relaxed Potential Energy Surface Scan of CH_3CN (ACN) and ACN^-

A CH_3CN molecule can not directly bind an excess electron in gas phase, as evidenced by its negative adiabatic electron affinities (AEA) of -0.42 eV calculated at the B3LYP/6-311++G(d,p) level. However, given the CPCM mode of the liquid acetonitrile phase, it can bind an excess electron either using $–CH_3$ Rydberg orbital with AEA of 0.92 eV or using –CN π* orbital with AEA of 1.39 eV. Thus, it can be concluded that: i) solvation effect significantly enhance the electron affinity of the CH_3CN molecule; ii) bending vibrations and stretching vibrations can increase its ability in binding EE, indicating that CH_3CN could be a potential captor of an excess electron.

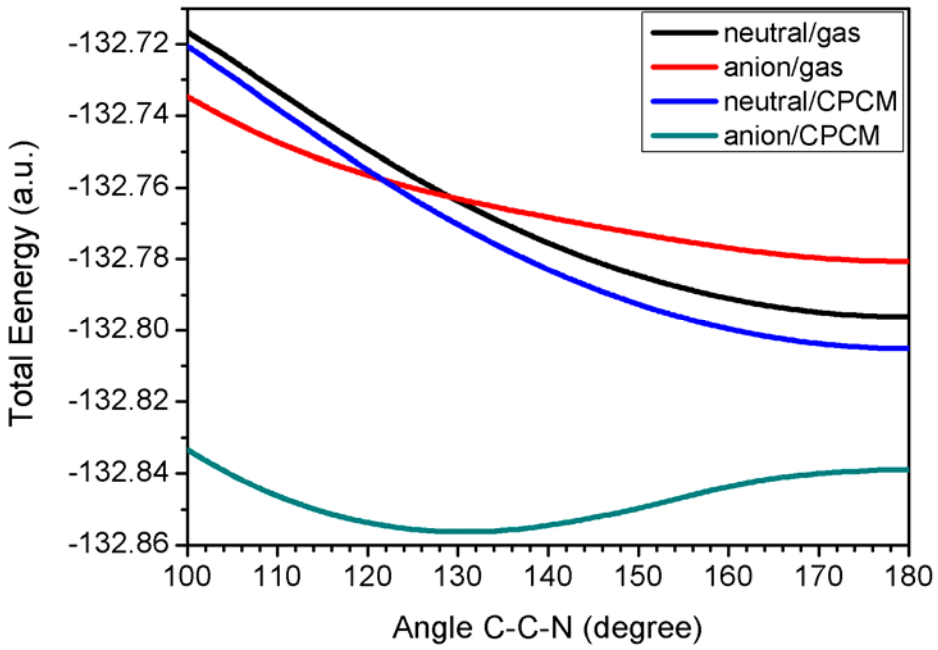

Figure S1. The scanned potential energy curves of neutral and anionic CH_3CN as a function of the C-C-N angle in the gas phase and in liquid acetonitrile (using the CPCM model) calculated at the B3LYP/6-311++G(d,p) level of theory.

3. Geometry Optimizations of the Negatively Charged ACN Clusters, (ACN_n^-) (n=2-30)

To prepare the ACN_n^- clusters with an interior *dimer anion*, a *cavity-shaped solvated electron*, and *a quasi-dimer core state*, respectively, we used the following procedure:

(i) To construct *liq*ACN with a *dimer anion*, a dimer anion with C_{2h} symmetry was firstly optimized at the BLYP/DNP level. The central C-C distance and ∠CCN were optimized to be 1.702 Å and 127.7°, respectively. Then, a *liq*ACN system was constructed by adding the optimized dimer anion and 120 acetonitrile molecules in a cubic simulation box with a density of 0.764 g/cm^3.

To construct *liq*ACN with a *cavity-trapped solvated electron*, a cavity was firstly constructed with the CH groups pointing toward the center. After geometry optimization of 2-6 ACN molecules, the cavity-trapped solvated electrons were formed with different cavity shape depending on the number of ACN molecules. Then, a *liq*ACN system was constructed by adding the cavity (surrounding by 6 ACN molecules) and 120 ACN molecules in a cubic simulation box with a density of 0.764 g/cm^3.

Similarly, to construct *liq*ACN with *a quasi-dimer core state*, a quasi-dimer was firstly optimized. ∠CCN of two molecules was optimized to be 129.4° and 175.6°, respectively, and the distance of H atom to central C atom of other molecule was 2.15 Å. Then, a *liq*ACN system was constructed by adding the optimized quasi-dimer and 120 ACN molecules in a cubic simulation box with a density of 0.764 g/cm^3.

(ii) The *liq*ACN systems were allowed to evolve at 300 K by the classical molecular dynamics simulation for 10 ps in the canonical ensemble. COMPASS force field was applied and the time step was set to 1.0 fs. For simulations all the spatial positions of atoms constructing a *dimer anion*, a *cavity-shaped solvated electron* and *a quasi-dimer core state* in the simulation box were fixed.

(iii) After equilibration, two independent configurations were extracted from the trajectory as the initial configuration of the ACN_n^- clusters, which contains a *dimer anion*, a *cavity-shaped solvated electron* or *a quasi-dimer core state*, respectively, and the nearby several other ACN molecules. Then, the ACN_n^- clusters, (n=2-30), were optimized at the BLYP/DNP level within the unrestricted open-shell scheme using DMol^3 package. All the spatial positions of atoms were unconstrained.

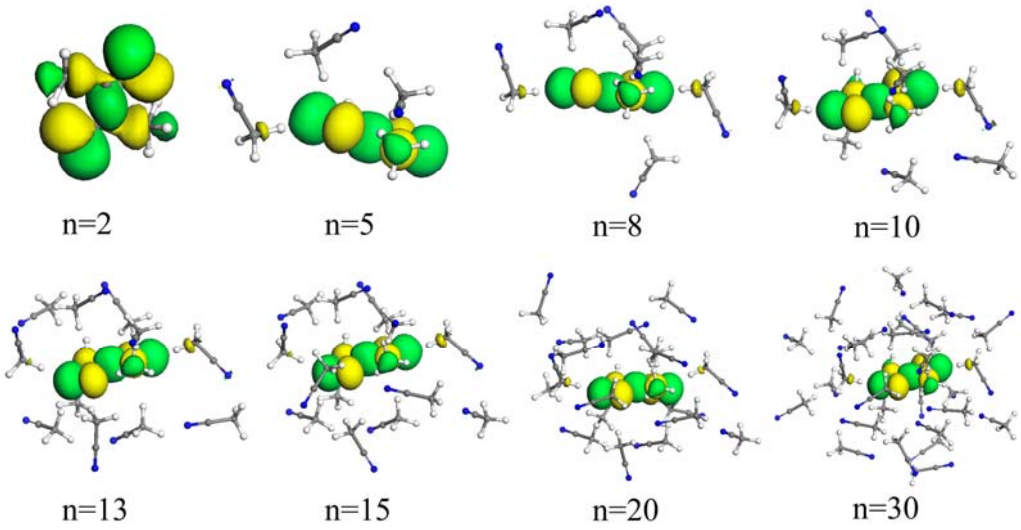

Figure S2. Optimized geometries of the negatively charged ACN clusters, (ACN_n^-) (n=2-30), within *a dimer anion state* at the BLYP/DNP level. The singly occupied molecular orbitals (SOMO) are shown with an isosurface value of 0.03. An excess electron is localized at a dimer core in each case.

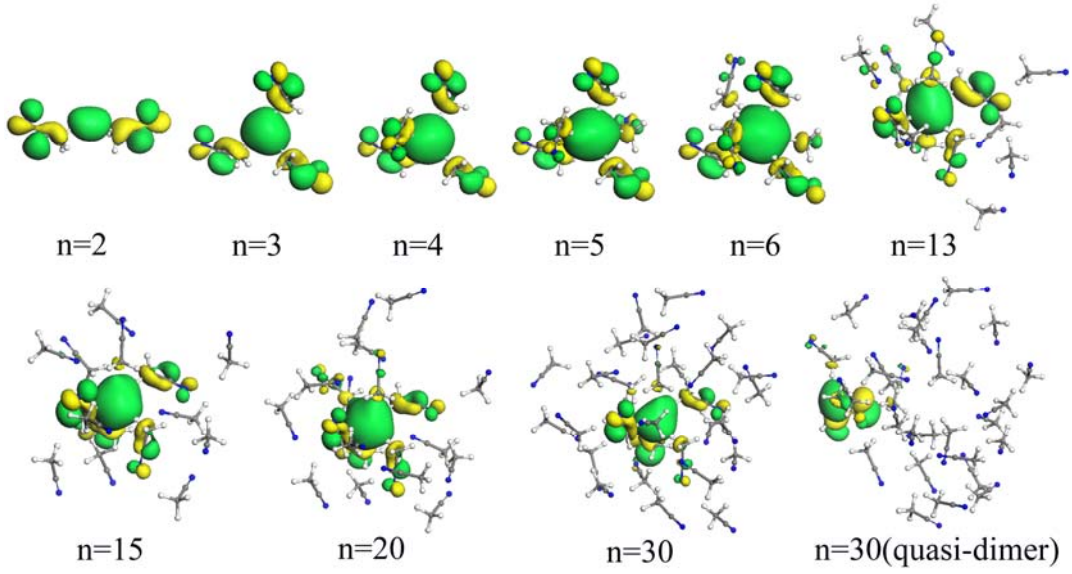

Figure S3. Optimized geometries of the negatively charged ACN clusters, (ACN_n^-) (n=2-30), within *a cavity-shaped solvated electron* at the BLYP/DNP level of theory. The singly occupied molecular orbitals (SOMO) are shown with an isosurface value of 0.03. An excess electron is localized in a cavity in each case, and however, *a quasi-dimer core state* can form in a large cluster (n=30).

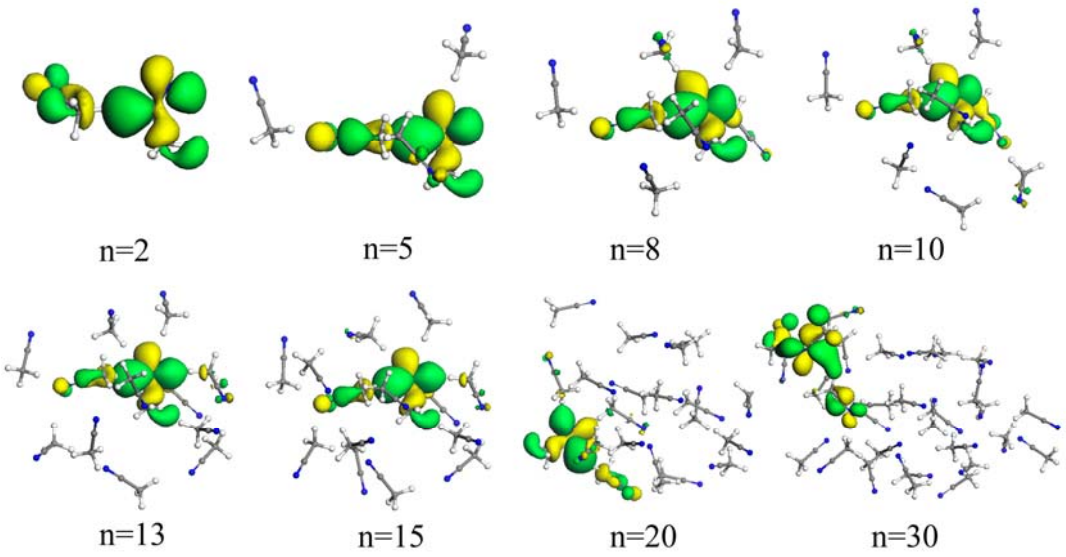

Figure S4. Optimized geometries of the negatively charged ACN clusters, (ACN_n^-) (n=2-30), within *a quasi-dimer core state* at the BLYP/DNP level of theory. The singly occupied molecular orbitals (SOMO) are shown with an isosurface value of 0.03. An excess electron is localized in a *quasi-dimer* core in each case, and however, *a quasi-dimer core state* can newly form at the surface of a large cluster (n≥20).

4. Optical Absorption Spectra and Vertical Detachment Energy (VDE) of the Optimized Negatively Charged ACN Clusters, (ACN_n^-) (n=2-30)

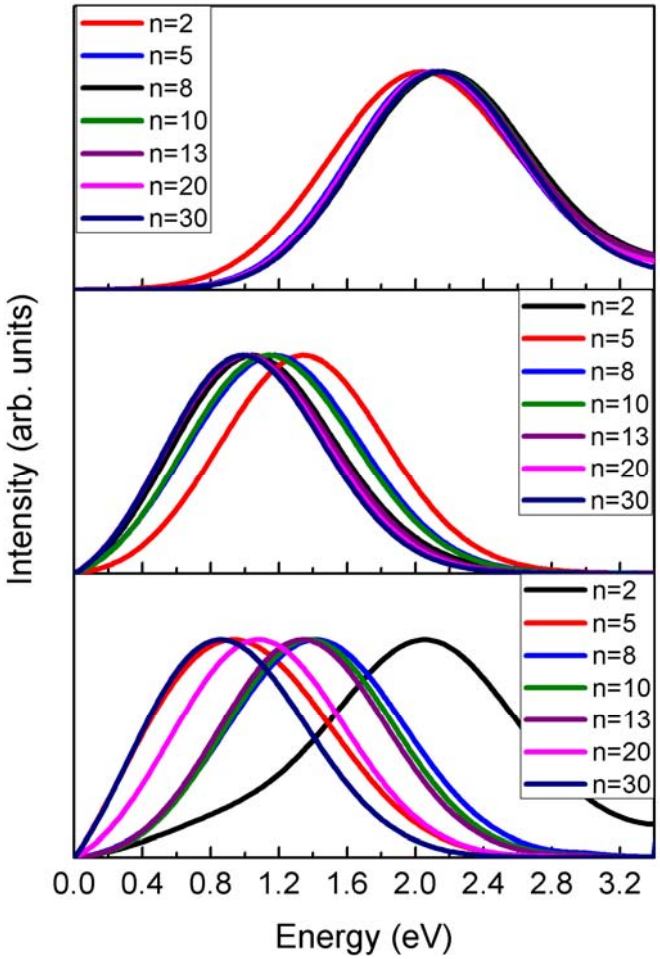

Figure S5. Optical absorption spectra of the ACN_n^- clusters with an interior *dimer anion* (top panel), a *cavity-shaped solvated electron* (middle panel), and *a quasi-dimer core state* (bottom panel), respectively.

Table S1. Vertical detachment energies (VDE) for the negatively charged ACN clusters, (ACN_n^-) (n=2-30), optimized at the BLYP/DNP level of theory. Values in the bracket are other initial optimized configurations from the classical molecular dynamics trajectory.

n	**VDEs (eV)**			
	dimer anion		*cavity-shaped solvated electron*	*quasi-dimer core state*
2	1.21	1.85 [a]	-0.52	0.10
3	1.34 (1.52)	2.34 [a]	-0.44	0.52 (0.46)
4	1.84 (2.00)	2.79 [a]	-0.05	0.67 (0.53)
5	2.16 (2.30)	3.13 [a]	0.28	0.60 (0.51)
6	2.49 (2.55)	3.43 [a]	0.51	1.06 (0.94)
7	2.80 (2.74)		0.54 (0.60)	1.17 (1.06)
8	3.07 (2.85)	3.85 [a]	0.56 (0.64)	1.22 (1.39)
10	3.05 (3.06)	4.22 [a]	0.79 (0.68)	1.60 (1.69)
13	3.21 (3.38)		0.62 (0.75)	1.83 (1.84)
15	3.27 (3.33)		0.86 (0.96)	1.95 (1.89)
20	3.39 (3.44)		0.88 (1.02)	2.08 (2.16)
30	3.63 (3.60)		1.21 (2.17 [b])	2.11 (2.27)

[a] The values are from Ref. [*Chem. Phys.* **2006**, *324*, 679-688], which were calculated at the B3LYP/6-31+G(d,p) level of theory. [b] The value indicates that an excess electron localizes in a *quasi-dimer* core rather than in a cavity.

Table S2. The calculated energies for the most stable negatively charged ACN clusters, (ACN_n^-) (n=2-30), optimized at the BLYP/DNP level of theory.

n	Calculated Total and Relative Energies (a.u.)			
	dimer anion		*cavity-shaped solvated electron* [c]	*quasi-dimer core state* [c]
2	-265.4868	-265.5381 [a]	0.0234	0.0015
3	-398.2486	-398.3127 [a]	0.0104	0.0012
4	-531.0238	-531.0850 [a]	0.0096	0.0057
5	-663.7947	-663.8565 [a]	0.0496	0.0184
6	-796.5622	-796.6321 [a]	0.0096	0.0017
7	-929.3298		0.0145	0.0118
8	-1062.1015	-1062.1760 [a]	0.0162	0.0091
10	-1327.6236	-1327.7213 [a]	0.0090	0.0034
13	-1725.9306		0.0203	0.0046
15	-1991.4628		0.0161	0.0064
20	-2655.3050		0.0365	0.0059
30	-3982.9498		0.0203 (0.0161 [b])	0.0161

[a] The values are from Ref. [*Chem. Phys. 324, 679-688, (2006)*], which were calculated at the B3LYP/6-31+G(d,p) level of theory. [b] The value indicated an excess electron localizes in a *quasi-dimer* core rather than localizes in a cavity. [c] For the cavity-shaped solvated electron and quasi-dimer core state, the values are the energies relative to the dimer anion for the corresponding cluster sizes calculated at the BLYP/DNP level of theory.

5. AIMD Simulations of the Neutral and Negatively Charged ACN Molecules

AIMD simulations were performed for the neutral and negatively charged ACN molecules at 300 K. Spin unrestricted calculations were carried out for 3.0 ps in canonical ensemble with time step of 1.0 fs. Temperature was controlled by Nosé-Hoover chain of thermostats. The generalized gradient corrected functional BLYP and numerical DNP basis set confined within a cutoff of 3.7 Å were used in the AIMD simulations. The electrostatic potential was evaluated by solving Poisson's equation with cutoff optimization in a completely numerical approach for the charge density.

The ∠CCN oscillates between 160° and 180° for neutral molecule, and oscillates between

110° and 137° for the negatively charged molecule. The corresponding average values are 172° and 124°, respectively.

Furthermore, the oscillation periods are 41-58 fs and 76-106 fs for a neutral and a negatively charged molecule, respectively, and the corresponding average periods are ~48.4 fs and ~89.7 fs, respectively.

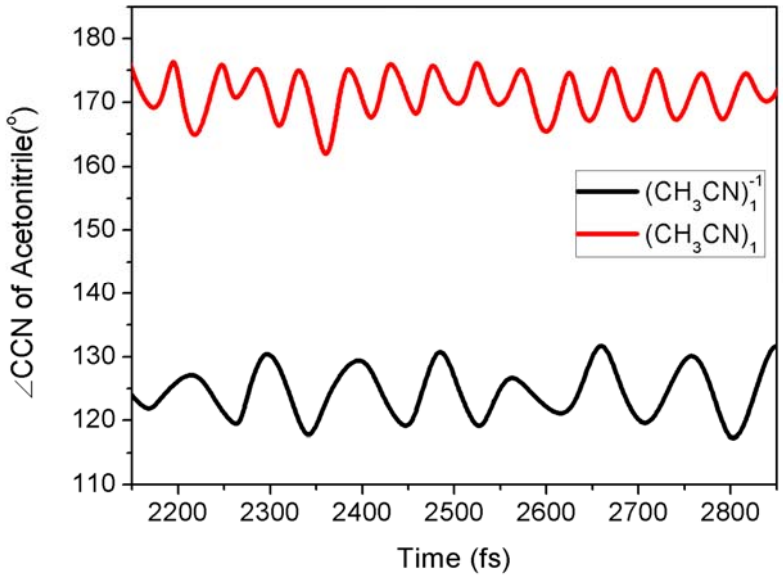

Figure S6. Oscillation of the ∠CCN bending vibration for an ACN molecule with (black line) and without (red line) an excess electron.

6. AIMD Simulations of the Negatively Charged ACN Clusters, (ACN_n^-) (n=5-30)

AIMD simulations were performed for the negatively charged ACN clusters, (ACN_n^-) (n =5, 10, 15, 20, 30), at 300 K using DMol[3] package. Spin unrestricted calculations were carried out for 1.0 ps in canonical ensemble with a time-step of 1.0 fs. The spin multiplicity was set to doublet and the total charge was set to -1. Temperature was controlled by Nosé-Hoover chain of thermostats. The generalized gradient corrected functional BLYP and numerical DNP basis set confined within a cutoff of 3.7 Å were used in the AIMD simulations. The electrostatic potential was evaluated by solving Poisson's equation with cutoff optimization in a completely numerical approach for the charge density.

After about 100 fs, the excess electron was localized in a *quasi-dimer*. For n≤15, ∠CCN decreases to about 135º within 100 fs, and then fluctuates about this value; for n=20, ∠CCN of two ACN molecules exhibit that one's loss is other's gain; for n=30, ∠CCN fluctuates between 150º and 173º.

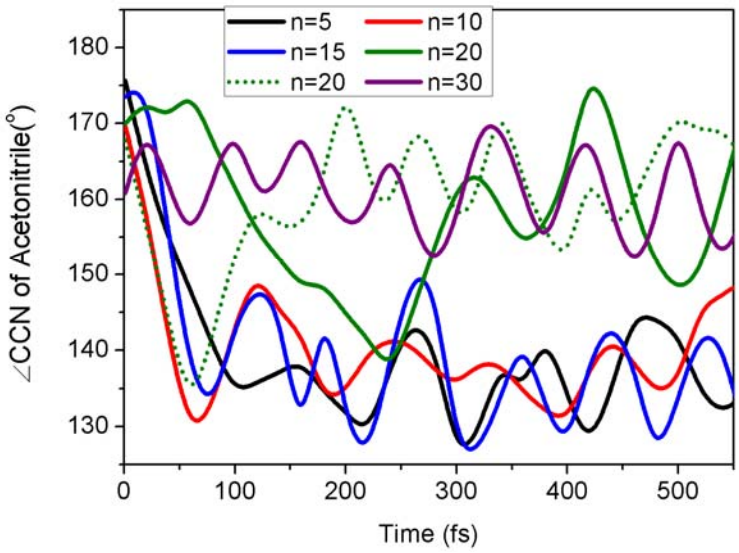

Figure S7. Time evolution of ∠CCN of the cored ACN molecule (*quasi-dimer core state*) in (ACN_n^-) (n=5, 10, 15, 20, 30) after AIMD simulations at 300 K.

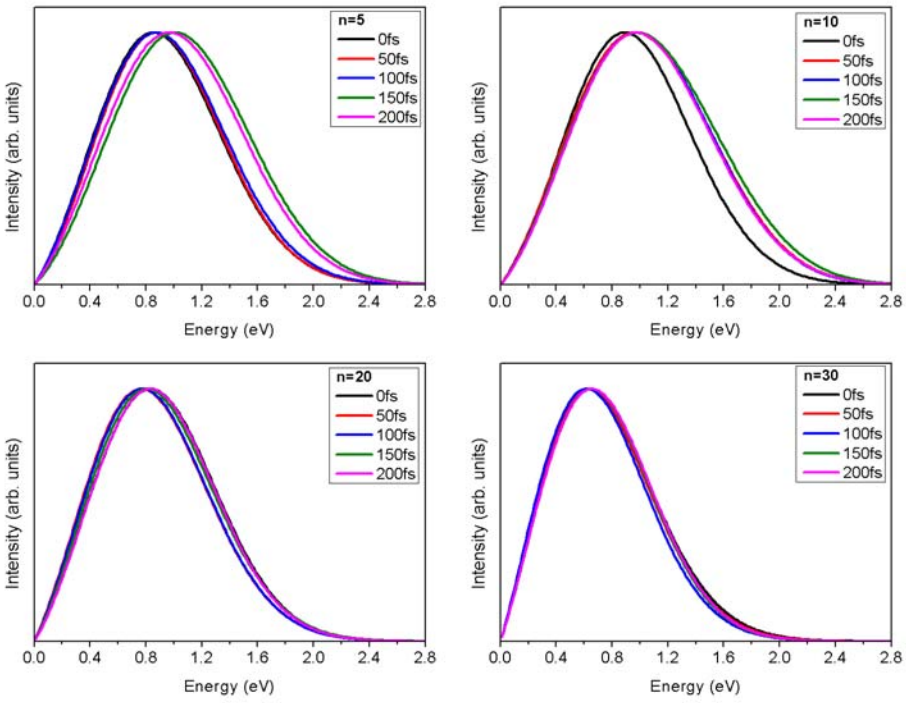

Figure S8. Optical absorption spectra of the negatively charged ACN clusters, (ACN_n^-) (n =5,

10, 20, 30) from the AIMD simulation trajectory at the times of 0, 50, 100, 150, and 200 fs.

7. Characteristics of the Lowest Unoccupied Molecular Orbitals of the Neutral *liq*ACN

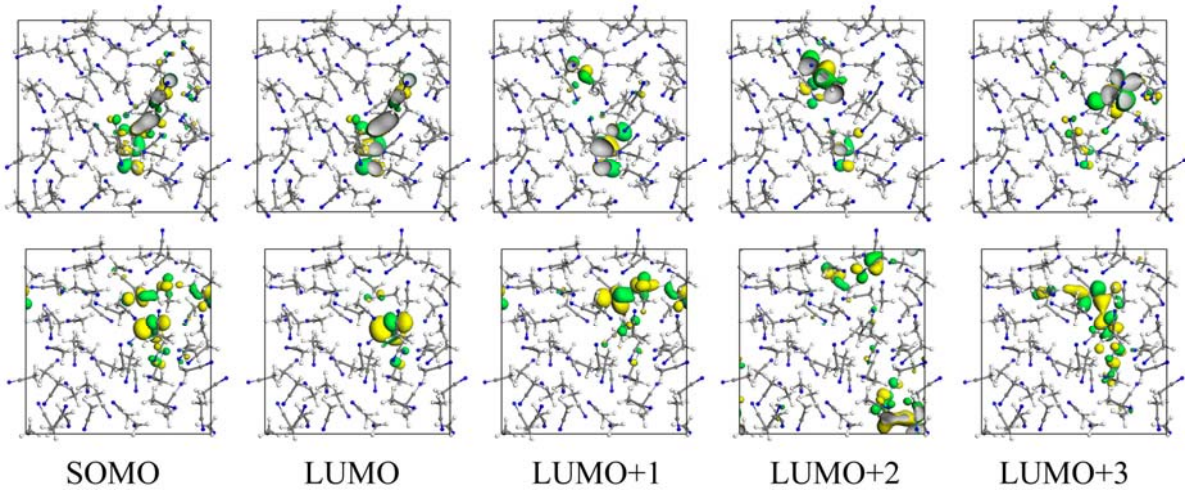

Figure S9. Several lowest unoccupied molecular orbitals (LUMOs) of two snapshot configurations of neutral *liq*ACN, as well as the corresponding singly occupied molecular orbital (SOMO) after vertically binding an excess electron.

8. Structural and Dynamic Properties of the Neutral and Negatively Charged *liq*ACN

We analyzed structural and dynamical properties of the neutral and negatively charged liquid acetonitrile. The radial distribution functions (RDFs) of carbon and nitrogen, carbon and carbon, and nitrogen and hydrogen are shown in Figure S10. The peaks corresponds to: (i) three peaks of Figure S10(a) are the intramolecular central C–N distance (~1.17 Å), intramolecular methyl C–N distance (~2.63 Å), and intermolecular C–N distance (~3.53 Å), respectively; (ii) two peaks of Figure S10(b) are the intramolecular central C–C distance (~1.48 Å), and intermolecular C–C distance (~4.17 Å), respectively; (iii) two peaks of Figure S10(c) are the intramolecular central N–H distance (~3.18 Å), and intermolecular N–H distance (~4.26 Å), respectively. The mean-square displacement (MSD) of liquid acetonitrile is shown in Figure S11, and the diffusion constant is about $3.0–3.8\times10^{-5}$ cm^2/s. These results agree well with the previous simulations and experiments (*J. Phys. Chem. B* **2006,** *110,* 3614-3623; *J. Chem. Soc., Faraday Trans. 1***, 1982**, *78*, 2233-2238), implying that we do a

truly equilibrated simulation.

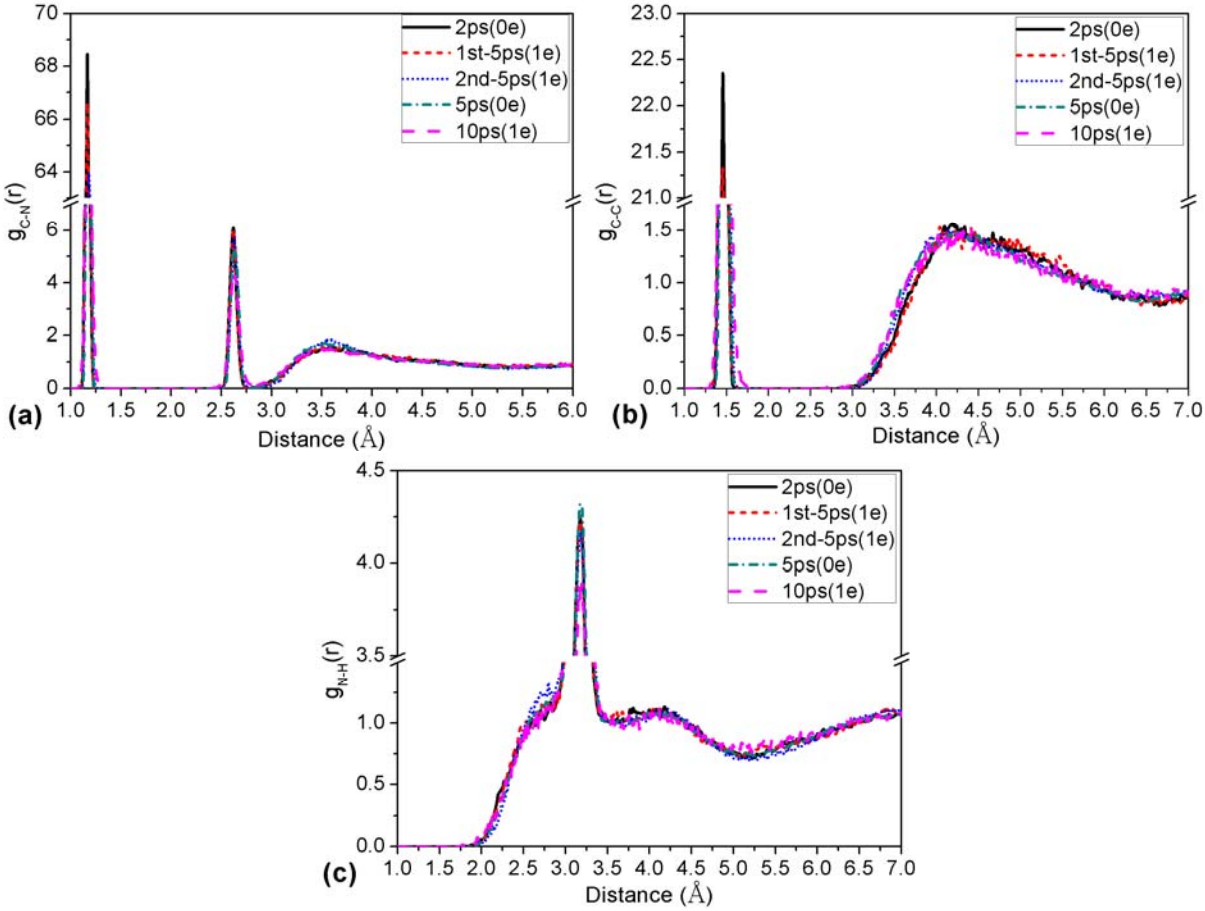

Figure S10. The radial distribution functions (RDFs) of carbon and nitrogen (a), carbon and carbon (b), and nitrogen and hydrogen (c). 2ps(0e), 1st-5ps(1e), and 2nd-5ps(1e) indicate the original 2.0-ps simulation of the neutral system, the original and extended 5.0-ps simulation of the negatively charged system, respectively. 5ps(0e) and 10ps(1e) indicate the 5.0 ps simulation of the neutral system with a different configuration and the 10 ps simulation of the negatively charged system, respectively.

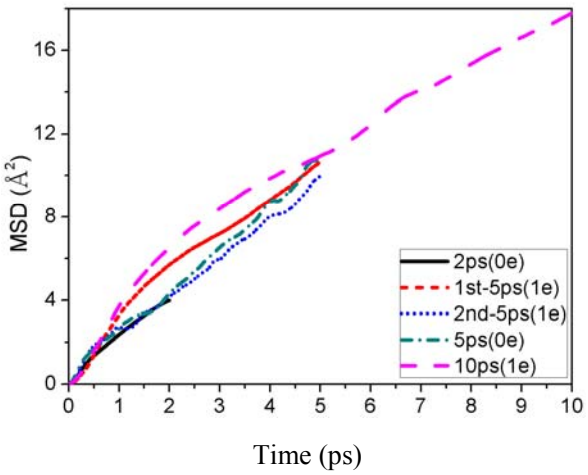

Figure S11. The mean-square displacement of the liquid acetonitrile. 2ps(0e), 1st-5ps(1e), and 2nd-5ps(1e) indicate the original 2.0-ps simulation of the neutral system, the original and extended 5.0-ps simulation of the negatively charged system, respectively. 5ps(0e) and 10ps(1e) indicate the 5.0 ps simulation of the neutral system with a different configuration and the 10 ps simulation of the negatively charged system, respectively.

9. Another Breathing Periods and Core-switching Shift Migration at Arbitrary Time Intervals from the Trajectory.

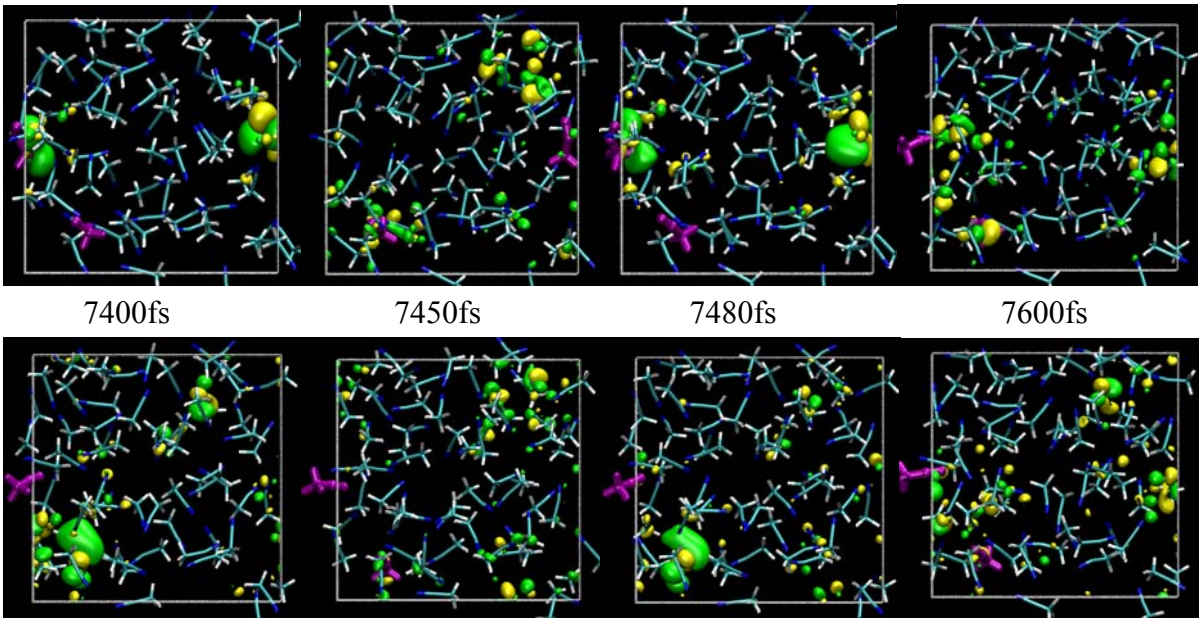

Figure S12. SOMO characters of representative snapshots extracted from the extended AIMD trajectory. Two breathing periods are shown in time scale of 7400–7480 fs and 7700–7790 fs, while a core-switching shift migration occurs at 7480–7700 fs.

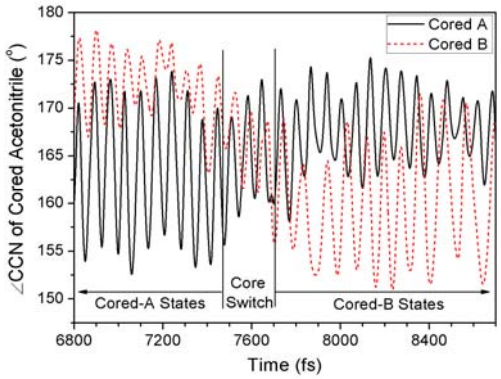

Figure S13. Oscillation of the ∠CCN bending vibration for two arbitrary ACN molecules (**A**/black curve and **B**/red curve) that are the cores, in turn, which bind the EE as localized states. The core-switching occurs at 7480-7700 fs that corresponds to the transfer of the EE from the **A**- to the **B**-cored localized state.

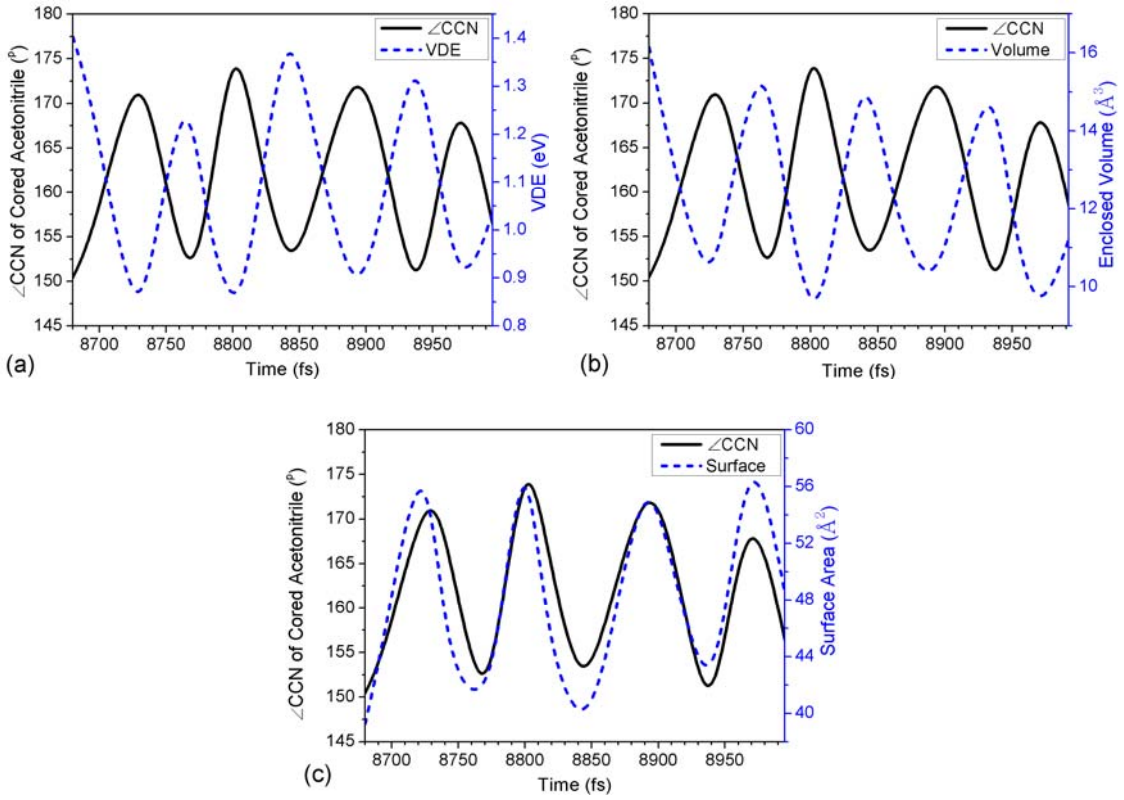

Figure S14. Oscillation behavior of the VDE (a), volume (b), and surface area (c) of the SOMO lobes enclosed by the 0.03-isovalued surface for the EE in *liq*ACN in an arbitrary time period (8680-8995 fs), and their cooperative relationship with the ∠CCN angle change.

10. A Different Initial Configurations of Excess Electron Solvation in liqACN for Reproduction of the Observed Phenomena

To investigate the effect of the initial configuration, we reconstructed the liquid acetonitrile and performed the following equilibrations: (i) The system was equilibrated by a 8.0-ns classical molecular dynamics simulation; (ii) the system was further equilibrated by a 5.0-ps *ab initio* molecular dynamics simulation; (iii) one 0-eV excess electron was vertically

injected and the system was simulated by *ab initio* molecular dynamics method for 10.0-ps. These simulations lead to the similar conclusions with the previous ones, as shown in Figures S15-S17.

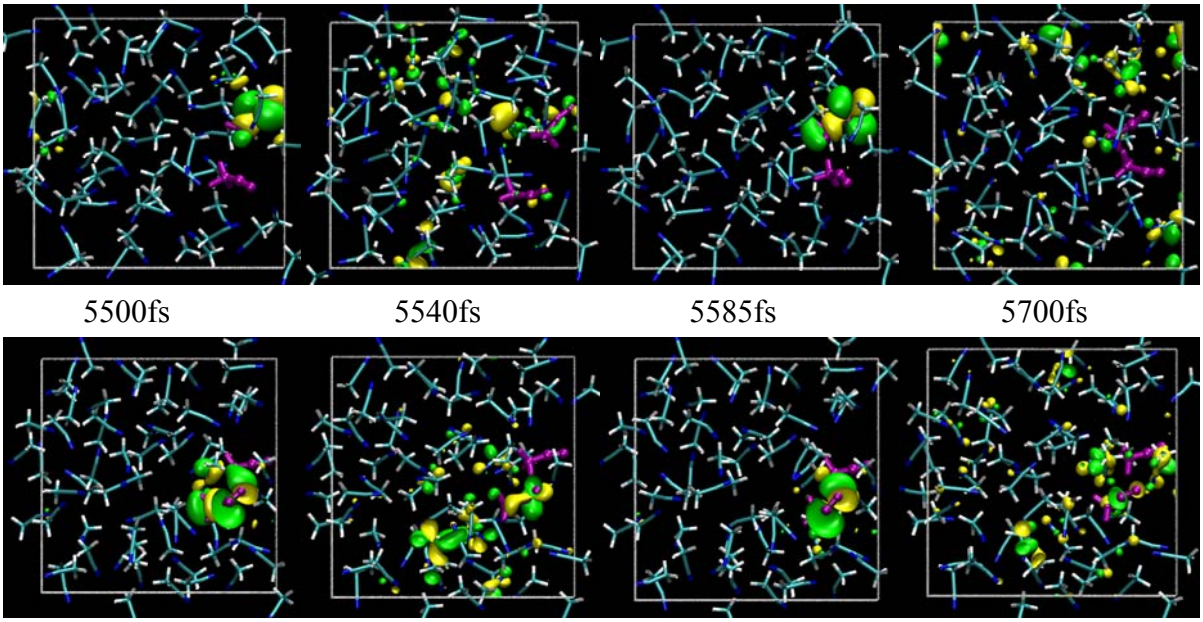

Figure S15. SOMO characters of representative snapshots extracted from the extended AIMD trajectory. Two breathing periods are shown in time scale of 5500-5585 fs and 5840-5930 fs, while a core-switching shift migration occurs at 5585-5840 fs.

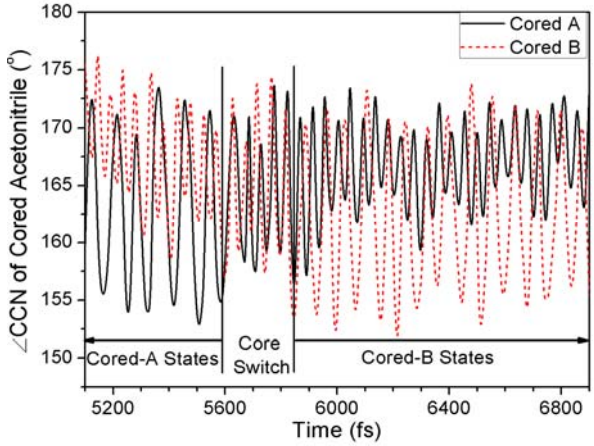

Figure S16. Oscillation of the ∠CCN bending vibration for two arbitrary ACN molecules (**A**/black curve and **B**/red curve) that are the cores, in turn, which bind the EE as localized states. The core-switching occurs at 5585-5840 fs that corresponds to the transfer of the EE from the **A**- to the **B**-cored localized state.

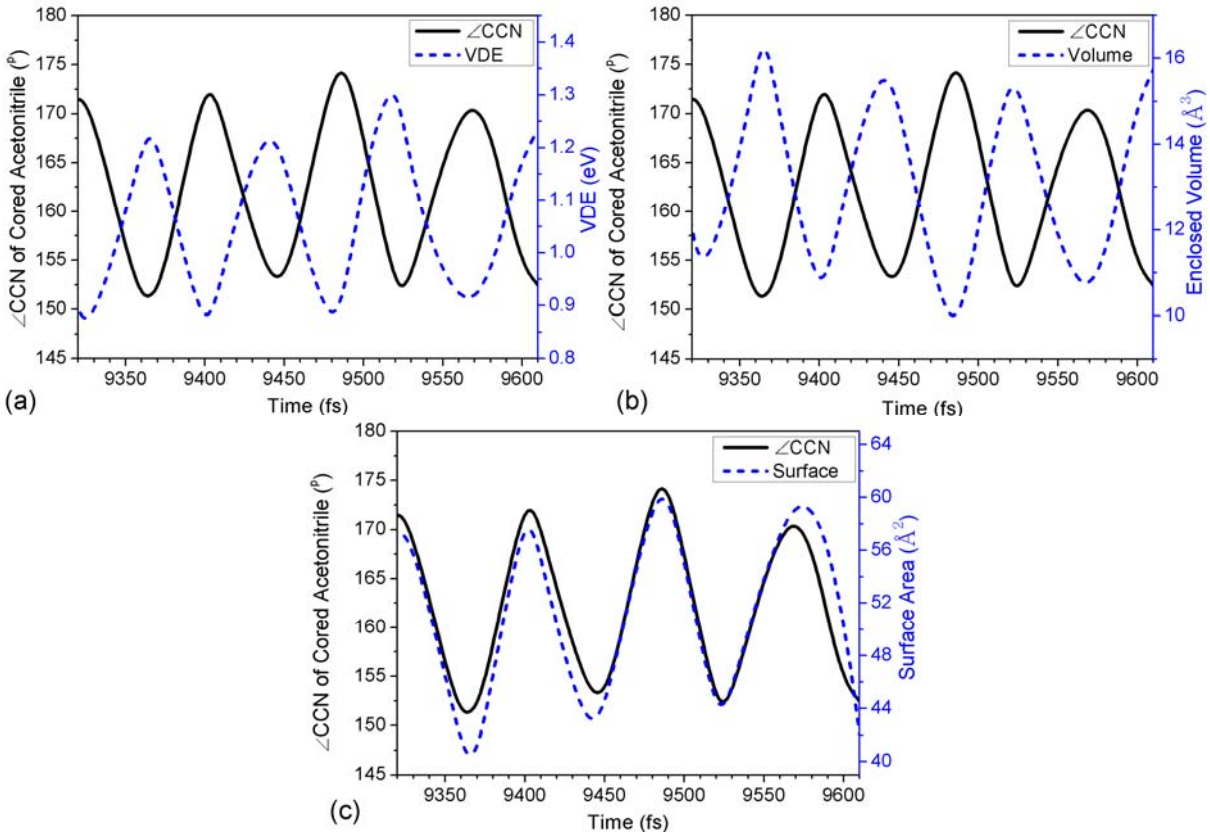

Figure S17 Oscillation behavior of the VDE (a), volume (b), and surface area (c) of the SOMO lobes enclosed by the 0.03-isovalued surface for the EE in *liq*ACN in an arbitrary time period (9320-9610 fs), and their cooperative relationship with the ∠CCN angle change.

11. AIMD-Simulated Results of an Excess Electron in *liq*ACN in a Larger Box (Size Effect)

To investigate the effect of the box size, we simulated a system consisting of 100 ACN molecules (cell parameter 20.8Å). We used the same simulation parameters described in the manuscript. The dynamics evolution of the excess electron was similar. Upon injection into the neutral solution, the excess electron was delocalized on several solvent. At ~130 fs the excess electron was localized on a bending solvent molecule (∠CCN≈153^{o}), forming *quasi-dimer core state*. Then ∠CCN of the cored ACN molecule periodically oscillates between 177^{o} and 150^{o}, corresponding the diffusely solvated state and localized state (quasi-dimer core state) of an excess electron.

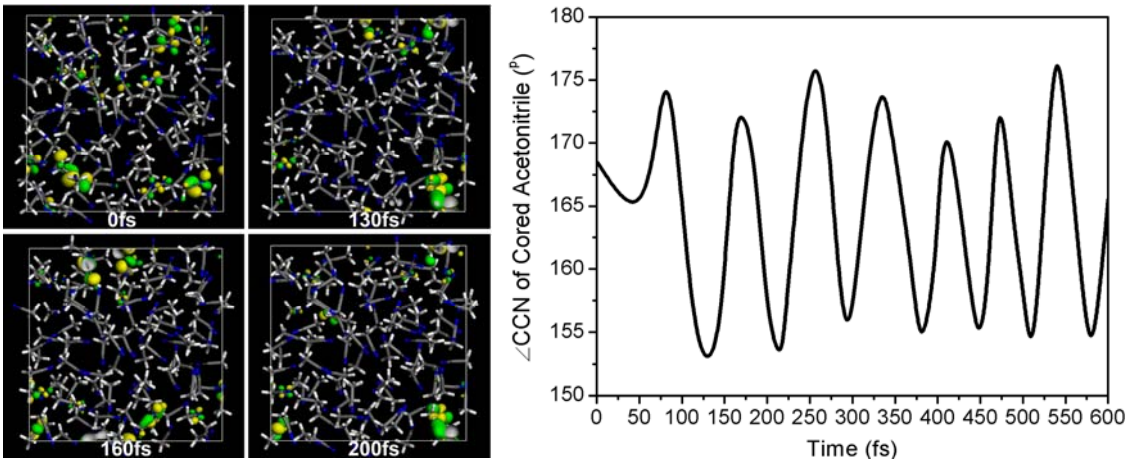

Figure S18. Snapshots of the singly occupied molecular orbital (SOMO, isovalue=0.03) and time evolution of ∠CCN of the cored ACN molecule from the trajectory.

12. Self-interaction Correction (SIC) for AIMD Simulations of an Excess Electron in *liq*ACN

In order to check the possible self-interaction error (SIE), we repeated our simulations using CP2K/Quickstep software package. The BLYP functional combined triple-zeta valence and polarization (TZVP) basis set and auxiliary plane waves were used to describe the valence states. The energy cutoff of plane waves was 300 Ry. The core states were described by the Goedecker-Teter-Hutter pseudopotential. The total ground state energy of the systems was minimized by the iterative self-consistent field (SCF) procedure using the orbital transformation method with *ASPC* extrapolation (K=3). The SCF tolerance was set 10^{-6}. Simulations were carried out in the canonical (NVT) ensemble using a timestep of 1.0 fs. Nosé-Hoover chain thermostats of length 3 were attached to every degree of freedom, with a time constant of 100 fs to ensure thermal equilibrium over the entire simulation trajectory. We simulated additional trajectories at 300K using the self-interaction correction methods (a=b=0.2) within a restricted open shell Kohn-Sham scheme [*Phys. Chem. Chem. Phys.* **7,** *1363 (2005)*]. However, SIE caused little effect on the dynamics and structure of the excess electron. On the other hand, results obtained from CP2K software without SIC was similar to the results obtained by the DMol[3] software.

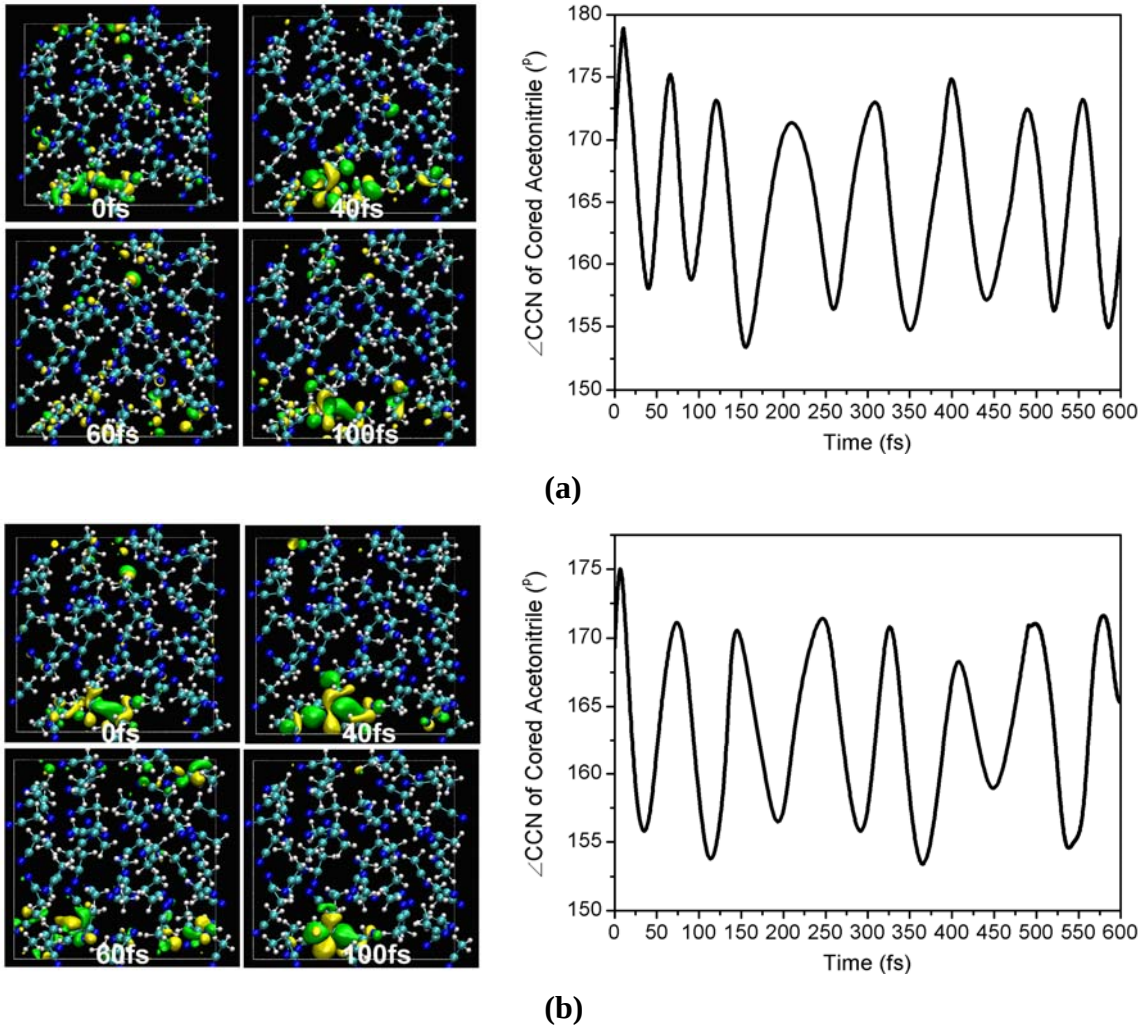

Figure S19. Snapshots of the singly occupied molecular orbital (SOMO, isovalue=0.02) and time evolution of ∠CCN of the cored ACN molecule from the CP2K trajectories without (**a**) and with (**b**) SIC.

13. Effects of the Dispersion Interactions and Basis Set on Dynamic Process of an Excess Electron in *liq*ACN

We perform additional AIMD simulation using the Quickstep/CP2K program package, and the long-range electron correlations that are responsible for van der Waals forces are described by the additional dispersion corrections to the normal XC functionals (*J. Comput. Chem.* **2006,** *27*, 1787-1799). Energies and forces are evaluated using BLYP exchange-correlation functional, with dispersion interactions accounted for using empirical pairwise damped London terms. The Goedecker-Teter-Hutter norm-conserving

pseudopotentials are employed. To evaluate the basis set effect, two basis sets have been tested: a triple-zeta plus *p*-type polarization basis set (TZVP), and a molecularly optimized basis set which contracts diffuse primitives with tighter valence orbitals (molopt-TZV2P). In agreement with the results obtained at the double numerical plus polarization (DNP) basis set that is comparable to the 6-31G** basis set, the dynamic process of an excess electron is still dominated by the quasi-dimer core state in the solvated state in liquid acetonitrile. Furthermore, the dispersion interaction has little effect on the structures and dynamics of an excess electron.

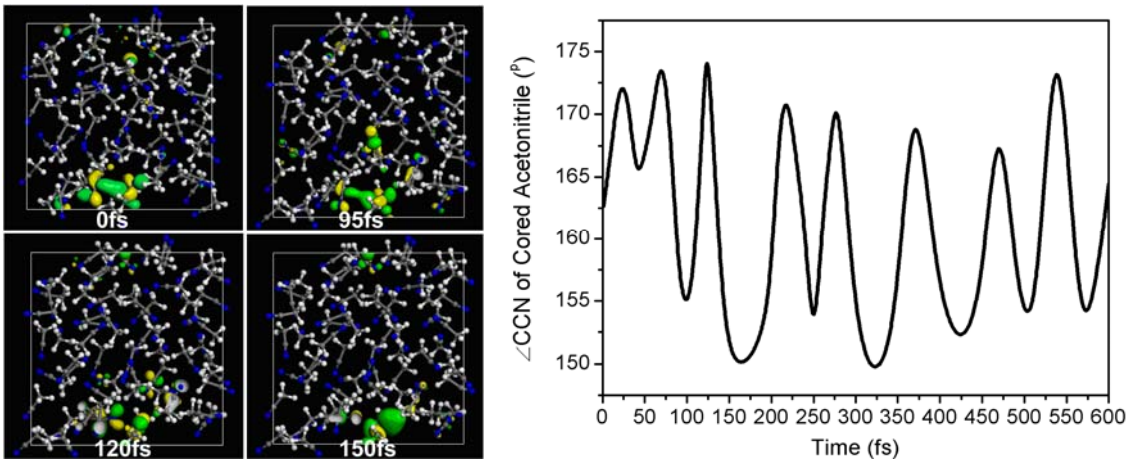

(a)

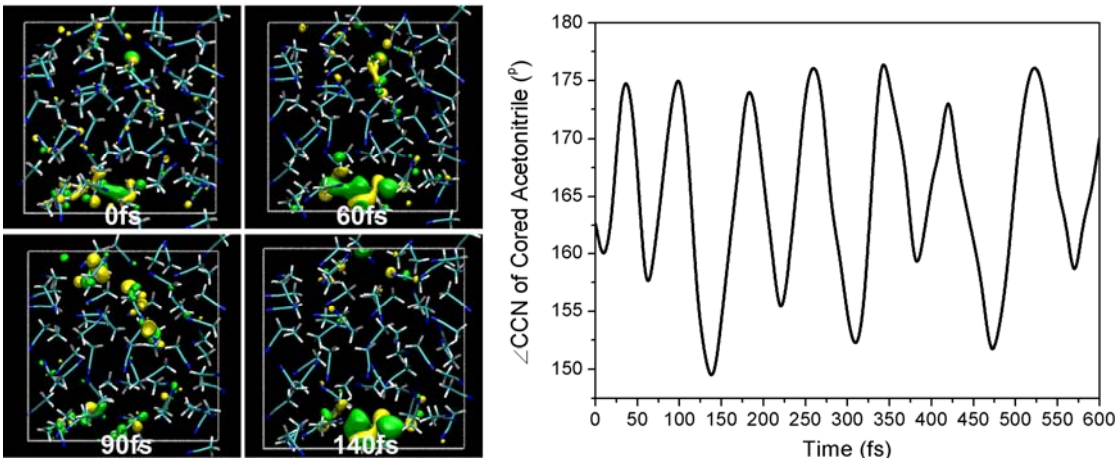

(b)

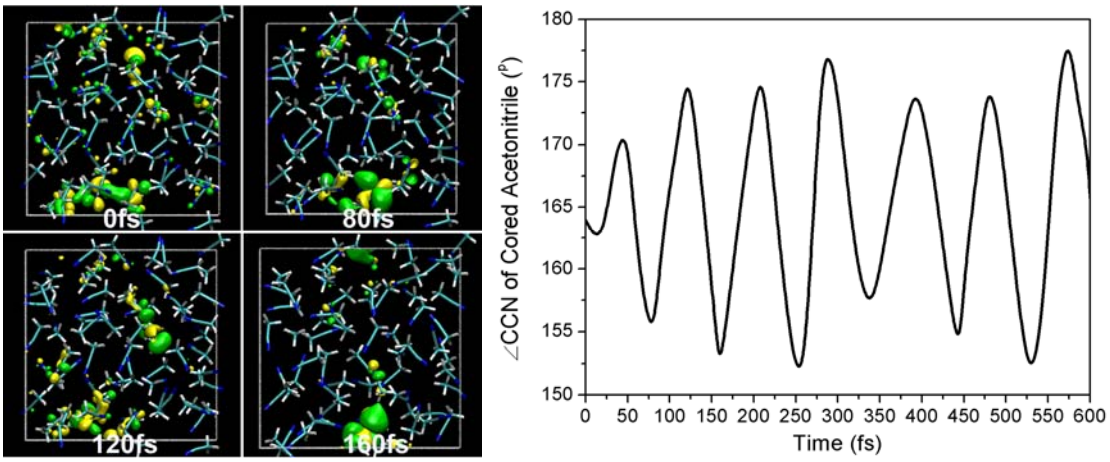

(c)

Figure S20. Snapshots of the singly occupied molecular orbital (SOMO, isovalue=0.03) and time evolution of ∠CCN of the cored ACN molecule AIMD-simulated using three methods: (a) BLYP/DNP, (b) BLYP/TZVP, and (c) BLYP/molopt-TZV2P. The latter two basis sets are performed by the CP2K software.

14. AIMD Simulations of an Excess Electron in *liq*ACN from the Starting Point of a Dimer Core State

To investigate the stability of the *dimer core states*, a *liq*ACN system containing *a dimer core state* is constructed by the following procedures: **i)** a dimer anion is optimized; **ii)** a cubic simulation box of density 0.764 g/cm^3 is constructed by adding the optimized dimer anion and other 62 ACN molecules; **iii)** the position of the dimer anion is constrained and the system is equilibrated by the classical molecular dynamics simulations; **iv)** after equilibrating the system for 100-ps, one electron is vertically added into the system and the system is AIMD simulated for 3.0 ps; **v)** the atom position of the cavity is unconstrained and the system is further AIMD simulated.

Upon attachment to neutral *liq*ACN, the excess electron was initially localized on the dimer core with VDE of ~2.3 eV. The lifetime of the *dimer core state* constructed artificially was ~1150 fs. Then, the excess electron is localized on one core at ~1200fs, forming the *quasi-dimer core state*. Subsequently, the breathing behavior occurs.

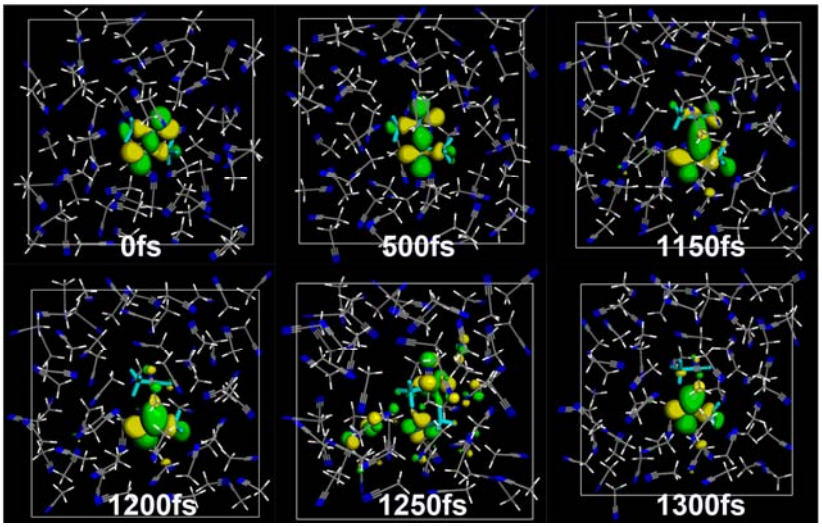

Figure S21. Snapshots from the AIMD trajectory at times 0, 500, 1150, 1200, 1250, and 1300 fs after well equilibrating the dimer anion in the *liq*ACN. The isovalue of the singly occupied molecular orbital (SOMO) is 0.03. The dimer molecules are shown in cyan stick style, and other molecules are shown in line style.

15. AIMD Simulations of an Excess Electron in *liq*ACN from the Starting Point of a Cavity-Shaped Solvated Electron State

To investigate the stability of the *cavity-shaped state*, a *liq*ACN system containing *a cavity-shaped electron* was constructed by the following procedures: **i)** a cavity consisted of 5 ACN molecules is optimized; **ii)** a cubic simulation box of density 0.764 g/cm^3 is constructed by adding the optimized cavity and other 59 ACN molecules; **iii)** the cavity structure is constrained and the system is equilibrated using the classical molecular dynamics simulations; **iv)** after equilibrating the system for 100-ps, one electron is vertically added into the system and the system is AIMD simulated for 3.0 ps; **v)** the cavity structure is unconstrained and the system is further AIMD simulated.

Upon attachment to neutral *liq*ACN, the excess electron was initially localized in a cavity with VDE of ~0.86 eV. The lifetime of the *cavity-shaped state* constructed artificially was ~30 fs. After that, a *diffuse state* forms and maintains until the *quasi-dimer core state* occurs at ~100 fs. Subsequently, the breathing behavior occurs.

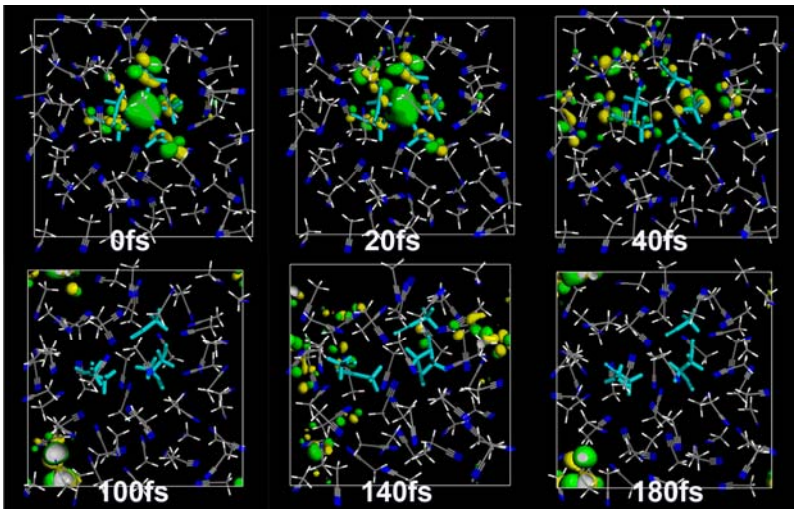

Figure S22. Snapshots from the AIMD trajectory at times 0, 20, 40, 100, 140, and 180 fs after well equilibrating the cavity-trapped solvated electron in liquid *liq*ACN. The isovalue of the singly occupied molecular orbital (SOMO) is 0.03. The cavity molecules are shown in cyan stick style, and other molecules are shown in line style.

16. Optical Absorption Spectra and Density of State of Various Observed States in *liq*ACN

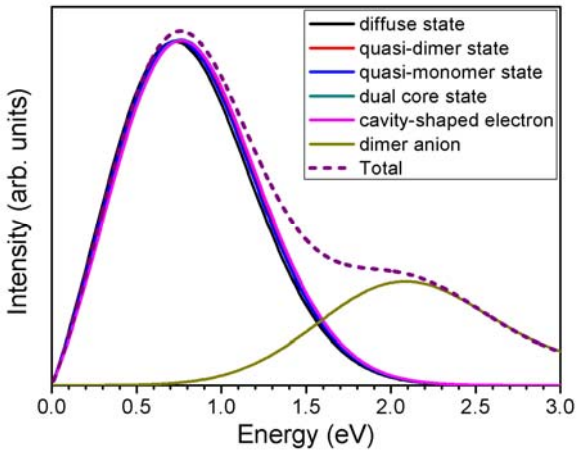

Figure S23. The calculated optical absorption spectra of various observed states of an excess electron in *liq*ACN along the AIMD simulation trajectory. The peaks of the adsorption spectra are at about 0.8 eV for the observed states including the diffusely solvated electron state, quasi-dimer state, quasi-monomer state, dual core state, and cavity-shaped solvated

electron state. These states correspond to the solvated electron state observed experimentally but with different structures. For the solvated dimer anion, the calculated absorption peak is at about 2.1 eV, in agreement with its experimental observation. In addition, the dashed line denotes a summed curve of the solvated electron state and the solvated dimer anion. Clearly, the distributions of these absorption spectra are very similar to the experimentally observed ones in Ref. 42. Note that the solvated dimer anion is a prepared one, not an observed snapshot configuration in the AIMD simulation.

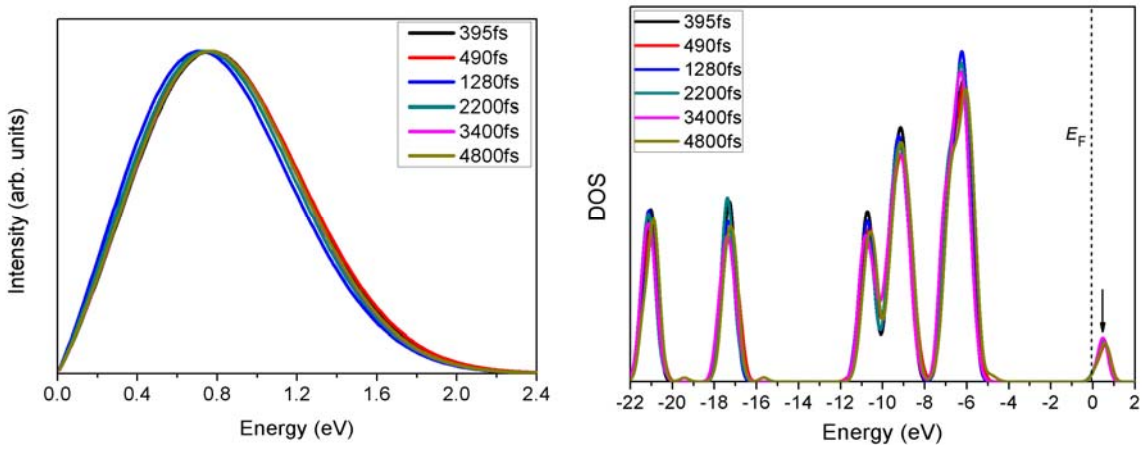

Figure S24. The calculated optical absorption spectra (left panel) and density of state (right panel) of the *quasi-dimer core state* of an excess electron in *liq*ACN at different times along the AIMD simulation trajectory.